J. Fluid Mech. (2005), *vol.* 522, *pp.* 91–100.
DOI: 10.1017/S0022112004001983 Printed in the United Kingdom

The lattice Boltzmann equation for natural convection in a two-dimensional cavity with a partially heated wall

By G. BARRIOS, R. RECHTMAN, J. ROJAS AND R. TOVAR

Centro de Investigación en Energía, UNAM, Apdo. Postal 34, Temixco, Morelos, 62580 Mexico
gbv@cie.unam.mx

(Received 28 June 2004 and in revised form 21 September 2004)

The lattice Boltzmann equation method in two dimensions was used to analyse natural convective flows. The method was validated with experiments in an open cavity with one of the vertical walls divided into two parts, the lower part conductive, the upper part and all the other walls adiabatic. An upward thermal boundary layer formed near the conductive wall. This layer gave way to a wall plume. The numerical results compared well with experiments in the laminar ($Ra = 2.0 \times 10^9$) and transition ($Ra = 4.9 \times 10^9$) regimes. The behaviour of the starting plume was numerically studied for Rayleigh numbers Ra from 10^6 to 4.9×10^9. The wall plume grows in three stages: in the first with constant acceleration, in the second with constant ascending velocity and in the third with negative acceleration due to the presence of the top boundary layer. The acceleration of the first stage and the velocity of the second both scale with the Rayleigh number.

1. Introduction

The lattice Boltzmann equation (LBE) method has proved in recent years to be a valuable computational fluid dynamics method (Benzi, Succi & Vergassola 1992; Chen & Doolen 1998; Succi 2001). The origin of this method lies in the lattice gas cellular automata (Hardy, de Pazzis & Pomeau 1976; Frisch, Hasslacher & Pomeau 1986; Doolen 1990). In these models the particles move synchronously in a discrete set of directions defined by the geometry of a lattice. It can be shown that the averaged occupation numbers, that is the ensemble-averaged distribution function, obey a Boltzmann's transport equation and that the averaged density and velocity satisfy similar equations to those of Navier–Stokes (Frisch *et al.* 1987). The LBE method recognizes that Boltzmann's transport equation is a computational tool that can be solved on the lattice (Higuera, Succi & Benzi 1989; Higuera & Jiménez 1989; Chen, Chen & Matthaeus 1992). The collision term of this equation can be simplified using the Bhatnagar, Gross, Krook (BGK) approximation (Bhatnagar, Gross & Krook 1954) where the distribution function relaxes to a local equilibrium with a constant relaxation time (Chen *et al.* 1992; Koelman 1991; Qian, d'Humieres & Lallemand 1992).

The LBE method has been successfully employed in the computational solution of problems with mass and momentum conservation. Problems where energy transport plays a dominant role are still a challenge (Succi 2001), although there have been interesting propositions beginning with those of Massaioli, Benzi & Succi (1993)

and Benzi *et al.* (1994). A concise review of the different methods for dealing with temperature can be found in Lallemand & Luo (2003*a*, *b*).

This paper deals with the application of the LBE method to the formation and development of a wall plume in a cavity with a partially heated wall. The problem of energy transport is approached by using two coupled fields, one for the distribution of particles and another for the temperature (Shan 1997; Buick & Greated 1998; Inamuro *et al.* 2002).

Turner (1962) discussed a model of starting free plumes generated by a local source of buoyancy that combines a front thermal or vortex ring with a steady turbulent plume solution. Experimental analysis of laminar starting free plumes has been carried out by Shlien & Boxman (1981), Moses, Zocchi & Libchaber (1993) and Kaminski & Jaupart (2003). Moses *et al.* found a constant ascending plume velocity while Kaminski & Jaupart found that the formation of the plume can be divided in three stages depending on the heat source distance. Both studies found that the ascending velocity scales with a power law of the Rayleigh number. Wall plumes are a particular case of thermal plumes as discussed by Sangras, Dai & Faeth (2000). They have been experimentally studied by Tovar, Rojas & Cedillo (2004).

The paper is divided as follows. Section 2 presents the LBE method with energy transport and introduces a body force and boundary conditions. The experimental setup and the relevant dimensionless parameters and quantities needed for its description are discussed in § 3. This is followed by the validation of the numerical method and the analysis of the starting wall plume for Rayleigh numbers in the range of 10^6 to 4.9×10^9. Some concluding remarks are presented in § 5.

2. The lattice Boltzmann equation

For energy transport, the LBE method is an iterative scheme where the cavity is a lattice and at each site of this lattice a set of particle and temperature distribution functions are defined. These distributions satisfy two coupled transport equations, which together with appropriate boundary and initial conditions lead to the solution of various heat transport phenomena and in particular natural convection in a partially heated cavity.

The particle distribution functions $f_i(\boldsymbol{r}, t)$ are defined as the probability of a particle being at a site $\boldsymbol{r}$ on a lattice at time t moving with velocity $\boldsymbol{c}_i$ with $i = 0, \ldots, b-1$. The b velocities are given by the symmetry of the lattice. In what follows the $D2Q9$ will be used. It is a two-dimensional square lattice where $b = 9$, $\boldsymbol{c}_0 = (0, 0)$, $\boldsymbol{c}_1 = (1, 0)$, $\boldsymbol{c}_2 = (0, 1)$, $\boldsymbol{c}_3 = (-1, 0)$, $\boldsymbol{c}_4 = (0, -1)$, $\boldsymbol{c}_5 = (1, 1)$, $\boldsymbol{c}_6 = (-1, 1)$, $\boldsymbol{c}_7 = (-1, -1)$, and $\boldsymbol{c}_8 = (1, -1)$. That is, particles can be at rest, moving along the axes to their nearest neighbour with speed 1 or along the diagonals to their next nearest neighbour with speed $\sqrt{2}$. In the BGK approximation, the particle distribution functions obey the transport equation

$$f_i(\boldsymbol{r} + \Delta t \boldsymbol{c}_i, t + \Delta t) - f_i(\boldsymbol{r}, t) = -\frac{\Delta t}{\tau}\left[f_i(\boldsymbol{r}, t) - f_i^{(eq)}(\boldsymbol{r}, t)\right], \tag{2.1}$$

where $i = 0, \ldots, b-1$, $\Delta t = 1$, τ is the relaxation time related to the viscosity and $f_i^{(eq)}$ is the local equilibrium distribution given by

$$f_i^{eq}(\boldsymbol{r}, t) = t_i \rho \left[1 + \frac{c_{i\eta} u_\eta}{c_s^2} + \frac{u_\eta u_\xi}{2c_s^2}\left(\frac{c_{i\eta} c_{i\xi}}{c_s^2} - \delta_{\eta\xi}\right)\right]. \tag{2.2}$$

In this expression ρ and $\boldsymbol{u}$ are the number density and velocity defined by

$$\rho(\boldsymbol{r},t)=\sum_{i=0}^{b-1} f_i(\boldsymbol{r},t), \qquad \boldsymbol{u}=\frac{1}{\rho}\sum_{i=0}^{b-1} f_i(\boldsymbol{r},t)\boldsymbol{c}_i, \tag{2.3}$$

and the subindices η and ξ denote the components of the vector quantities with the usual convention of a sum over repeated subindices. Also $t_i = 4/9$, $1/9$ and $1/36$ for $|\boldsymbol{c}_i| = 0$, 1 and $\sqrt{2}$ respectively and $\delta_{\eta\xi} = 1$ if $\eta = \xi$ and zero otherwise (Qian *et al.* 1992). Finally, $c_s = 1/\sqrt{3}$ is the speed of sound and the viscosity ν is related to the relaxation time by $\nu = c_s^2(\tau - \tau_0)$ with $\tau_0 = 1/2$. Since $\nu > 0$, $\tau > \tau_0$.

The temperature T is defined by

$$T(\boldsymbol{r},t)=\sum_{i=0}^{b-1} T_i(\boldsymbol{r},t) \tag{2.4}$$

where T_i are the temperature distribution functions that obey the transport equation

$$T_i(\boldsymbol{r}+\Delta t\boldsymbol{c}_i, t+\Delta t) - T_i(\boldsymbol{r},t) = -\frac{\Delta t}{\tau_T}\left[T_i(\boldsymbol{r},t) - T_i^{eq}(\boldsymbol{r},t)\right]. \tag{2.5}$$

In this expression, τ_T is the relaxation time for the temperature field and $T_i^{(eq)}$ is the local equilibrium temperature distribution given by

$$T_i^{eq}(\boldsymbol{r},t) = Tt_i[1 + 3\boldsymbol{c}_i \cdot \boldsymbol{u}]. \tag{2.6}$$

The temperature T satisfies a diffusion equation with a thermal diffusivity α given by $\alpha = c_s^2(\tau_T - \tau_0)$. Since $\alpha > 0$, $\tau_T > \tau_0$ (Guo, Shi & Zheng 2002).

Natural convection can be simulated by adding a body force g_i in the vertical direction y to equation (2.1) that has the form

$$g_i(\boldsymbol{r},t) = 3t_i g\beta(T(\boldsymbol{r},t) - T_0)c_{iy}. \tag{2.7}$$

In this expression c_{iy} is the vertical component of $\boldsymbol{c}_i$, g is the acceleration due to gravity in the lattice, β is the thermal expansion coefficient and T_0 a reference temperature. This body force does not contribute to the density but it does change momentum.

Finally, a way to implement boundary conditions on adiabatic and conductive walls must be specified. For the particle distribution functions a no-slip condition is used by simply reversing the direction of the incoming distributions at the walls, known as a bounce-back condition. Although other boundary conditions can also be used (Inamuro, Yoshino & Ogino 1995; Inamuro 2002), we found the bounce-back boundary conditions to be numerically stable. For the temperature distribution function, adiabatic walls are simulated by putting the temperature at the sites of the walls equal to the temperature at the nearest site inside the cavity. This guarantees a zero temperature gradient. On the other hand, the site in contact with the conductive wall assumes the specified temperature which, if needed, can change in time.

3. Experimental setup

The experimental cavity is shown schematically in figure 1. It is filled with water initially in thermal equilibrium at a temperature T_0. The top of the cavity is open to the atmosphere while the right and bottom walls are adiabatic. The left-hand wall is divided in two parts: the upper part is adiabatic while the lower is conductive (shown

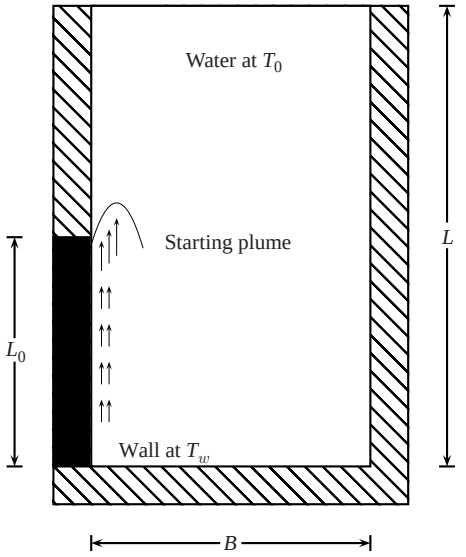

FIGURE 1. Schematic view of the cavity. The black zone represents the conductive heated wall, the rest of the walls are adiabatic and the top of the cavity is open to the atmosphere. The cavity has a breadth of 0.202 m and $B = 0.34$ m, $L = 0.65$ m and $L_0 = 0.36$ m.

in black in the figure). The front and back walls of the cavity are glass sheets that allow visualization of the convective flow using the schlieren technique (Tovar 2002). The experiment started when the conductive wall was heated externally; its temperature which was initially T_0 relaxed to T_w in the first few seconds of the experiment. An upward thermal boundary layer was formed near the conductive wall. This layer gave way to a wall plume with instabilities travelling upwards in the thermal boundary layer depending on the value of the Rayleigh number.

For natural convection the important dimensionless parameters are the Rayleigh Ra and Prandtl Pr numbers defined by

$$Ra = \frac{g\beta \Delta T L_0^3}{\alpha \nu} \quad \text{and} \quad Pr = \frac{\nu}{\alpha}, \tag{3.1}$$

where g is the acceleration due to gravity, β the thermal expansion coefficient, $\Delta T = T_w - T_0$, L_0 the characteristic length (the height of the conductive wall), α the thermal diffusivity, and ν the viscosity. For water $Pr = 6.2$.

A schlieren system with a laser light source, two parabolic mirrors of 0.7 m diameter and a high-resolution video camera was used to record the formation of the thermal boundary layer and the starting wall plume for $Ra_1 = 2.0 \times 10^9$, $Ra_2 = 4.9 \times 10^9$ and $Ra_3 = 9.2 \times 10^9$ that correspond to laminar, transition and turbulent regimes, respectively (Tovar *et al.* 2004).

The numerical simulations were performed in a two-dimensional version of the experimental cavity. The upper free surface of the experimental setup was replaced by a rigid wall at a constant temperature equal to the initial temperature T_0 of the fluid. In the LBE method $T \in [0, 1]$ so $T_0 \sim 0$. In the experiments the Rayleigh number was varied by changing ΔT and in the numerical simulations by changing L_0 keeping L_0/L and B/L fixed. The experimental and numerical results can be compared by

using the dimensionless quantities defined below with an asterisk:

$$x^* = \frac{x}{L}, \qquad y^* = \frac{y}{L}, \qquad t^* = t\frac{\alpha}{L_0^2}, \tag{3.2}$$

$$u^* = v\frac{L_0}{\alpha}, \qquad v^* = u\frac{L_0}{\alpha}, \qquad T^* = \frac{T - T_0}{T_w - T_0}. \tag{3.3}$$

In these expressions, (x, y) is the position of a point in the cavity measured in metres in the experiment and at lattice sites in the numerical simulations, t is time in seconds and in number of updating steps in the experiments and simulations respectively. Also u and v are the velocities in the x- and y-directions respectively and their units follow from the previous ones. Finally the temperature T is measured in degrees Kelvin in the experiment and is a number between 0 and 1 in the simulations. In what follows, we have chosen to present all the results in the more familiar units of the experiment.

4. Experiments and simulations

Numerical simulations were carried out, for the three Rayleigh numbers mentioned before, by iteratively solving equations. (2.1) and (2.5) on a $D2Q9$ finite lattice with the appropriate boundary conditions. At $t = 0$ homogeneous particle and temperature distribution functions with $\boldsymbol{u} = 0$ and T_0 were chosen and the conductive wall was then heated as follows. In the experiments, the temperature of the wall at $t = 0$ s was T_0 and then increased during the first few seconds to T_w. The data obtained from the thermocouples on the conductive wall can be fitted by an exponential relaxation from T_0 to T_w according to

$$T(l) = \begin{cases} T_0 & \text{if } t < t_0(l), \\ T_0 + (T_w - T_0)(1 - \exp[-(t - t_0(l))/\sigma]) & \text{if } t \geqslant t_0(l), \end{cases} \tag{4.1}$$

where $0 \leqslant l \leqslant L_0$ and σ is a relaxation time which together with t_0 may be found from the experimental data (Tovar 2002; Barrios 2003). In the numerical simulations, the initial temperature change in the conductive wall mimics the experiment; $T_0 \sim 0$, $T_w \sim 1$ and σ and t_0 are evaluated from the experimental data.

The isotherms found numerically are compared with the images obtained with the schlieren technique in the experiments for Ra_1 in figure 2. In (a) and (b) a slow thickening of the thermal boundary layer due to the gradual heating of the conductive wall can be observed. Fluid at a temperature T_0 is slowly incorporated into the lower part of the boundary layer. The incipient formation of the starting plume at $y = L_0$ can also be observed. The starting plume is characterized by an ascending vortex that grows with time. The numerical prediction of the vortex shape and position compares well with the experimental results. In the lower part of the vertical wall some travelling instabilities were observed. They are manifested as a local thickening of the thermal boundary layer in figure 2(g). For this Rayleigh number the numerical simulations were performed on a lattice of 1005×1895 sites which corresponds to a space resolution Δx (distance between nearest neighbour sites) of 3.38×10^{-4} m and a time resolution Δt of 3.15×10^{-3} s. Since the thermal boundary layer has an approximate thickness of 4×10^{-3} m it is satisfactorily resolved by the simulation.

A quantitative comparison between experiments and simulations can be obtained by following the topmost position of the wall plume. In the experiments, it is found from the analysis of the digitized images and the error is estimated to be of the order

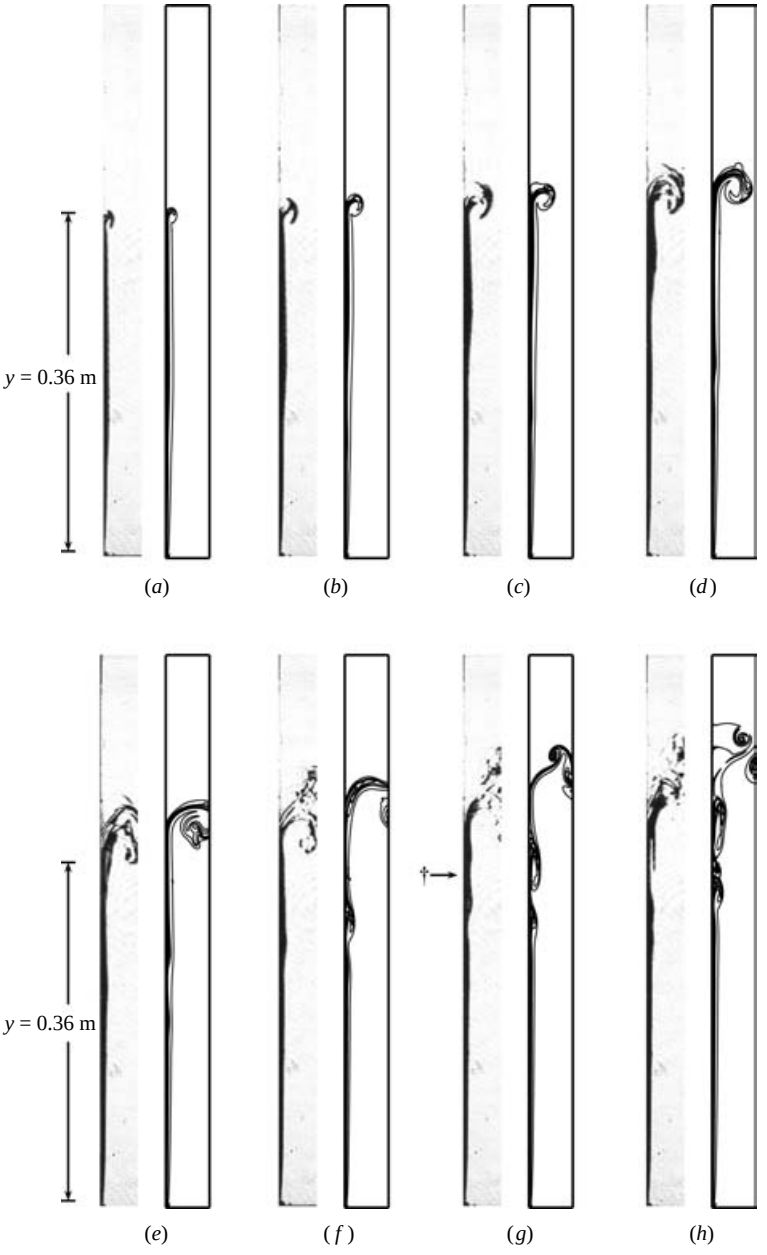

FIGURE 2. Schlieren images and isothermal lines for $Ra_1 = 2.0 \times 10^9$ in a box of height 0.6 m and width 0.05 m and (*a*) $t = 30$ s, (*b*) $t = 35$ s, (*c*) $t = 40$ s, (*d*) $t = 45$ s, (*e*) $t = 50$ s, (*f*) $t = 55$ s, (*g*) $t = 60$ s, and (*h*) $t = 65$ s. In each pair of frames, the left one was obtained experimentally with the schlieren technique and the one on the right numerically using the LBE. The isothermal lines are spaced $\Delta T^* = 0.1$. The † symbol in (*g*) indicates a travelling instability.

of 10^{-3} m and in the numerical simulations, it is the topmost position of the isotherm with temperature $1.01T_0$. The position of the topmost point of the thermal plume is shown in figure 3(*a*). The errors between the experimental results and the numerical results, defined as the maximum of the relative difference between the experimental

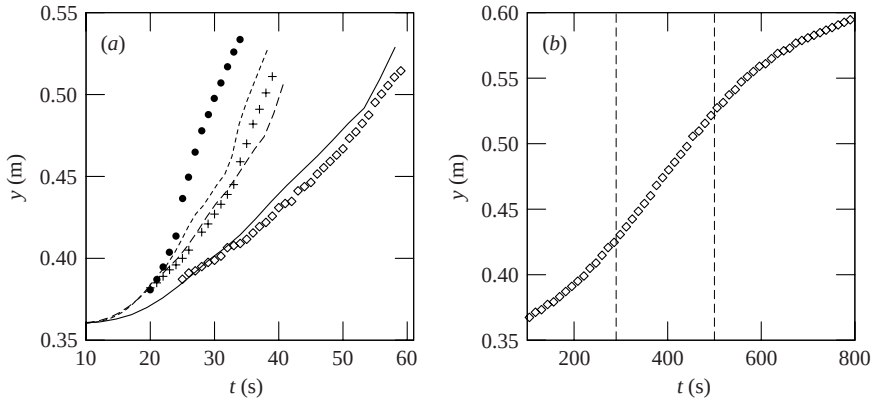

FIGURE 3. (*a*) Topmost vertical position of the wall plume. The experimental and numerical results for Ra_1 are shown by $\diamond$ and the full line respectively, for Ra_2 by $+$ and the dashed curve and for Ra_3 by $\bullet$ and the dotted curve. (*b*) Topmost vertical position of the wall plume as a function of time for $Ra = 1 \times 10^7$. The dashed vertical lines separate the three main stages.

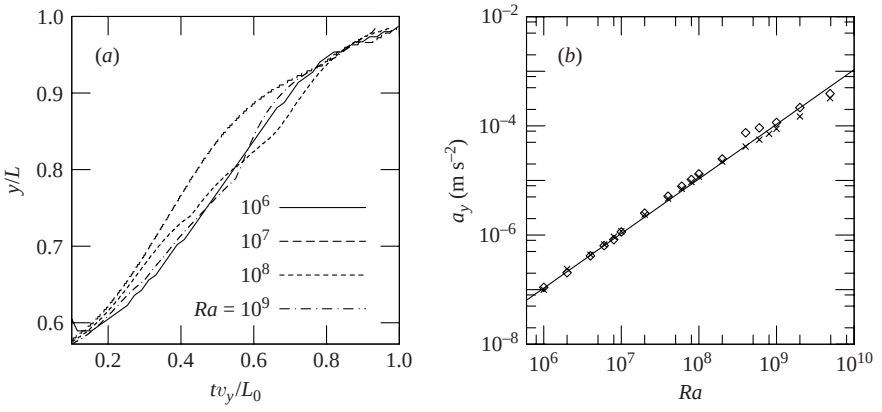

FIGURE 4. (*a*) Vertical growth scaled with the inverse of the height of the cavity as a function of the time scaled with the vertical velocity corresponding to the second stage of the plume and the inverse of the characteristic length. (*b*) Vertical acceleration a_y of the topmost position of the starting wall plume ($\diamond$) and of the thermal centre ($\times$) as a function of Ra. Both accelerations obey scaling relations with $\alpha = 1.06 \pm 0.01$ and $\alpha = 0.964 \pm 0.004$ for the former and the latter respectively. The solid line corresponds to $\alpha = 1$.

and numerical value with respect to the experimental one, are not greater than 3.8%, 6.9% and 10.7% for Ra_1, Ra_2 and Ra_3 respectively. This indicates that the lattice Boltzmann method is a valid numerical scheme in the laminar and transition regimes and underestimates the experimental results in the turbulent regime.

The growth of the wall plume takes place in three stages as shown in figure 3(*b*) for $Ra = 10^7$. In the first stage the plume ascends with a constant acceleration which ends at about $t = 300$ s where a second stage with approximate constant velocity can be identified. The durations of these two stages are Δt_1 and Δt_2 respectively. In the third stage, due to the influence of the upper wall, a negative acceleration is present. This description agrees with that given by Kaminski & Jaupart (2003) for symmetrical plumes. In the first stage, the buoyancy force of the plume is greater than the viscous dissipation, while in the second they are balanced. In figure 4(*a*) the topmost vertical

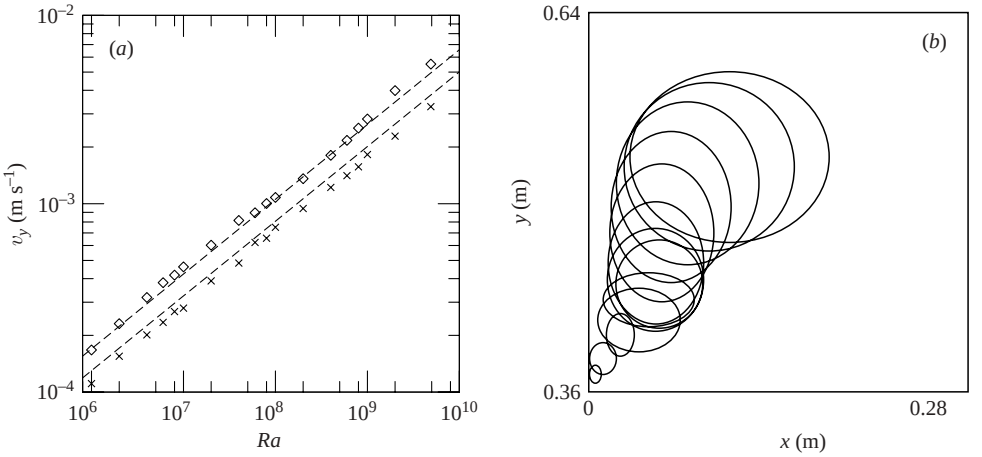

FIGURE 5. (*a*) Vertical velocity of the topmost position corresponding to the second stage of the starting wall plume (◇) and of its thermal centre (×) as a function of *Ra*. Both obey a scaling relation with $\beta = 0.399 \pm 0.005$ and $\beta = 0.0394 \pm 0.003$ for the former and the latter respectively, shown as curves. (*b*) A representation of the wall plume by ellipses obtained from a numerical simulation for Ra_1. The bottom left-hand corner is the point where the conductive wall meets the adiabatic wall. The ellipse nearest to the bottom represents the wall plume at $t = 30$ s, the other ellipses represent the plume at 5 s intervals.

position of the plume, scaled with the inverse of the total height of the cavity, as a function of time, scaled with the constant vertical velocity of the second stage and the inverse of L_0, is plotted for several Rayleigh numbers. The fact that the four cases considered almost collapse on a single curve is evidence that the vertical velocity during the second stage is of fundamental importance in the description of the phenomenon.

In analogy with the centre of mass of a body, the thermal centre $\boldsymbol{r}_{tc}$ is defined by

$$\boldsymbol{r}_{tc}(t) = \int_{A(t)} \boldsymbol{r} T(\boldsymbol{r}, t) \mathrm{d}^2\boldsymbol{r} \left[\int_{A(t)} T(\boldsymbol{r}, t) \mathrm{d}^2\boldsymbol{r} \right]^{-1} \tag{4.2}$$

where $A(t)$ is the area occupied by the plume at time t and $T(\boldsymbol{r}, t)$ is the temperature distribution at time t. This quantity can be readily found both in experiments and in numerical simulations and may furnish a better understanding of the wall plume. Higher moments can also be found. The vertical component of $\boldsymbol{r}_{tc}$ behaves qualitatively like the vertical position of the topmost part of the plume as shown in figure 4(*b*) for the acceleration in the first stage and in figure 5(*a*) for the velocity in the second stage. The vertical acceleration a_y scales with the Rayleigh number as $a_y \sim Ra^{\alpha}$ with $\alpha \sim 1$, and the vertical velocity v_y in the second stage also obeys a power law of the form $v_y \sim Ra^{\beta}$ with $\beta \sim 0.4$. Moses *et al.* (1993) found for a rising laminar symmetrical plume that $\beta = 0.5 \pm 0.1$ for several substances and in particular for water, $\beta \sim 0.4$. The duration of the first and second stages Δt_i, $i = 1, 2$ also obey power laws $\Delta t_i \sim Ra^{\gamma}$ with $\gamma \sim -1/2$.

The ascending vortex in the starting plume can be represented to first order by $\boldsymbol{r}_{tc}(t)$ and to second order as an ellipse centred around $\boldsymbol{r}_{tc}(t)$ with semi-axes $\sigma_x(t)$ and $\sigma_y(t)$, the standard deviations of the thermal centre in the x- and y-directions respectively. This simplified description is shown figure 5(*b*) where it is evident that the major semi-axis of the ellipse switches from the vertical to the horizontal directions in time.

5. Concluding remarks

The LBE approach used in this paper treats temperature as a field coupled with the particle distribution field. This is a simple way of dealing with temperature, although at the cost of doubling the number of distribution functions and the use of computer memory. Although other LBE schemes with energy transport can in principle be applied to the same problem (see Lallemand & Luo 2003*a* for a list of references) the agreement with the experimental results, the simplicity of the method and the possibility of doing simulations with large lattices seem to be sufficient to justify its usefulness.

It was found that the bounce-back boundary condition was numerically more stable than the method developed by Inamuro *et al.* (1995). The scheme used to set the temperature of the conductive wall was also found to be numerically stable and capable of setting the temperature as a function of time.

The LBE method captures qualitatively and quantitatively the dynamics of the wall plume. It is able to reproduce the travelling instabilities in the thermal boundary layer as shown in figure 2. The shape and position of the top cap of the starting wall plume obtained with the LBE method are in good agreement with experimental results using the schlieren technique. The time evolution can be separated in three stages. In the first, the formation of the wall plume, the acceleration of its topmost part and that of the thermal centre are similar and follow the same scaling behaviour. In the second stage, the vertical velocity of the topmost part of the rising plume is larger than that of the thermal centre due to the fact that in this stage the temperature distribution inside the plume $T(\boldsymbol{r}, t)$ plays an important role. However, both velocities show the same scaling behaviour. The thermal centre and its moments can be used to obtain information on the behaviour of the wall plume and can prove useful in other situations.

Stimulating discussions with E. Ramos are gratefully acknowledged. The comments and questions posed by one of the referees have enriched the contents of this paper. This work was supported in part by projects DGAPA-UNAM IN109602 and CONACyT U41347-F.

REFERENCES

Barrios, G. 2003 Estudio numérico de la convección natural usando la técnica de la ecuación de Boltzmann en redes. Master's thesis, UNAM.

Benzi, R., Succi, S. & Vergassola, M. 1992 The lattice Boltzmann equation: Theory and applications. *Phys. Rep.* **222**, 145–197.

Benzi, R., Tripiccione, R., Massaioli, M., Succi, S. & Ciliberto, S. 1994 On the scaling of the velocity and temperature structure functions in turbulent Rayleigh-Bénard convection. *Europhys. Lett.* **25**, 341.

Bhatnagar, P. L., Gross, E. P. & Krook, M. 1954 A model for collision processes in gases. i. small amplitude processes in charged and neutral one-component systems. *Phys. Rev.* **94**, 511–525.

Buick, J. M. & Greated, C. A. 1998 Lattice Boltzmann modeling of interfacial gravity waves. *Phys. Fluids* **10**, 1490–1511.

Chen, H., Chen, S. & Matthaeus, W. H. 1992 Recovery of the Navier–Stokes equations using a lattice-gas Boltzmann method. *Phys. Rev.* A **45**, R5339–R5342.

Chen, S. & Doolen, G. D. 1998 Lattice Boltzmann method for fluid flows. *Annu. Rev. Fluid Mech.* **30**, 329–364.

Doolen, G. D. (Ed.) 1990 *Lattice Gas Methods for Partial Differential Equations*. Addison Wesley.

Frisch, U., Hasslacher, B. & Pomeau, Y. 1986 Lattice-gas automata for the Navier-Stokes equation. *Phys. Rev. Lett.* **56**, 1505–1508.

Frisch, U., d'Humieres, D., Hasslacher, B., Lallemand, P., Pomeau, Y. & Rivet, J.-P. 1987 Lattice gas hydrodynamics in two and three dimensions. *Complex Systems* **1**, 649–707.

Guo, Z., Shi, B. & Zheng, C. 2002 A coupled lattice BGK model for the Boussinesq equations. *Intl J. Numer. Meth. Fluids* **39**, 325–342.

Hardy, J., de Pazzis, O. & Pomeau, Y. 1976 Molecular dynamics of a classical lattice gas: Transport properties and time correlation functions. *Phys. Rev.* A **13**, 1949–1961.

Higuera, F. J. & Jiménez, J. 1989 Boltzmann approach to lattice gas simulation. *Europhys. Lett*. **9**, 663–668.

Higuera, F. J., Succi, S. & Benzi, R. 1989 Lattice gas dynamics with enhanced collisions. *Europhys. Lett*. **9**, 345–349.

Inamuro, T., Yoshino, M. M., Inoue, H., Mizuno, R. & Ogino, F. 2002 A lattice Boltzmann method for a binary miscible fluid mixture and its application to a heat-transfer problem. *J. Comput. Phys*. **179**, 201–215.

Inamuro, T., Yoshino, M. & Ogino, F. 1995 A non-slip boundary condition for lattice Boltzmann simulations. *Phys. Fluids* **7**, 2928–2930.

Kaminski, E. & Jaupart, C. 2003 Laminar starting plumes in high Prandtl-number fluids. *J. Fluid Mech*. **478**, 287–298.

Koelman, J. M. 1991 A simple lattice Boltzmann scheme for Navier–Stokes fluid flow. *Eur. Phys. Lett*. **15**, 603–607.

Lallemand, P. & Luo, L. S. 2003*a* Hybrid finite-difference thermal lattice Boltzmann equation. *Intl J. Mod. Phys.* B **17**, 41–47.

Lallemand, P. & Luo, L. S. 2003*b* Theory of the lattice Boltzmann method: acoustic and thermal properties in two and three dimensions. *Phys. Rev.* E **68**, 036706.

Massaioli, F., Benzi, R. & Succi, S. 1993 Exponential tails in two–dimensional Rayleigh Bènard convection. *Europhys. Lett*. **21**, 305–310.

Moses, E., Zocchi, G. & Libchaber, A. 1993 An experimental study of laminar plumes. *J. Fluid Mech*. **251**, 581–601.

Qian, Y., d'Humieres, D. & Lallemand, P. 1992 Lattice BGK models for the Navier–Stokes equation. *Eur. Phys. Lett*. **17**, 479–484.

Sangras, R., Dai, Z. & Faeth, G. M. 2000 Velocity statistics of plane self-preserving buoyant turbulent adiabatic wall plumes. *J. Heat Transfer* **124**, 460–469.

Shan, X. 1997 Simulation of Rayleigh–Bénard convection using a lattice Boltzmann method. *Phys. Rev.* E **55**, 2780–2788.

Shlien, D. J. & Boxman, R. L. 1981 Laminar starting plume temperature fiel measurement. *J. Heat Mass transfer* **24**, 919–931.

Succi, S. 2001 *The Lattice Boltzmann Equation for Fluid Dynamics and Beyond*. Oxford University Press.

Tovar, R. 2002 Estudios sobre transición y turbulencia en flujos de convección natural. PhD thesis, DEPFI-UNAM.

Tovar, R., Rojas, J. & Cedillo, M. 2004 Development of a wall plume from a boundary layer along a partially vertical wall. *Intl Commun. Heat Mass Transfer* **31**, 561–571.

Turner, J. S. 1962 The starting plume in neutral surroundings. *J. Fluid Mech*. **13**, 356–368.